SOFT ROBOTS

A soft matter computer for soft robots

M. Garrad[1,2,3]*, G. Soter[1,2]*, A. T. Conn[2,4], H. Hauser[1,2], J. Rossiter[1,2]†

Despite the growing interest in soft robotics, little attention has been paid to the development of soft matter computational mechanisms. Embedding computation directly into soft materials is not only necessary for the next generation of fully soft robots but also for smart materials to move beyond stimulus-response relationships and toward the intelligent behaviors seen in biological systems. This article describes soft matter computers (SMCs), low-cost, and easily fabricated computational mechanisms for soft robots. The building block of an SMC is a conductive fluid receptor (CFR), which maps a fluidic input signal to an electrical output signal via electrodes embedded into a soft tube. SMCs could perform both analog and digital computation. The potential of SMCs is demonstrated by integrating them into three soft robots: (i) a Softworm robot was controlled by an SMC that generated the control signals necessary for three distinct gaits; (ii) a soft gripper was given a set of reflexes that could be programmed by adjusting the parameters of the CFR; and (iii) a two–degree of freedom bending actuator was switched between three distinct behaviors by varying only one input parameter. SMCs are a low-cost way to integrate computation directly into soft materials and an important step toward entirely soft autonomous robots.

INTRODUCTION

The next generation of robotic systems must be capable of safely operating in complex, dynamic environments. Integrating soft matter into the system is an elegant way of achieving this; by exploiting the inherent compliance of soft materials, robots that adapt to—rather than resist—the environment can be developed (*1*–*4*). This insight has driven recent interest in soft robotics, leading to the development of soft matter actuation (*5*–*8*), sensing (*9*–*12*), and power (*13*–*15*) systems. However, far less attention has been paid to the development of soft matter mechanisms for computation. The range and complexity of behaviors that can be created using only materials-based control approaches are limited, and as a result, soft robotic systems have until now mostly been controlled by electronic microcontrollers. A better approach for soft matter systems could be to build a soft matter computational system directly into the body of the robot. This would lead to a new generation of soft robots, with levels of autonomy similar to their rigid cousins, but without sacrificing the benefits associated with soft materials.

Here, we introduce the conductive fluid receptor (CFR) and show that it is a fundamental building block for a range of soft matter computers (SMCs). The SMC concept takes inspiration from the way in which the vascular system is used in biological systems to encode and transmit information that is processed locally in distinct organs. For example, hormones, such as adrenaline, are released into the bloodstream and disperse throughout the body. When detected by an appropriate receptor, hormones trigger a local response (e.g., increased blood flow in flight muscles and dilation of the pupils in the eyes). In a similar way, an SMC encodes information in the spatial structure of a fluidic tape that travels through the soft body. When this information is detected by an appropriate receptor, it generates an output. We show SMC architectures for performing both analog and digital computations and a number of ways in which these simple architectures can be composed to compute more complex functions. We further demonstrate that the outputs generated by an SMC can be connected directly to soft actuators and embedded within the body of a robot, creating a range of robots with integrated soft matter controllers.

To introduce a new computational mechanism, we must first consider what it means to do computation in this context. We follow the widely accepted definition from (*16*), which defines a computer to be a physical device that can be used to perform a mapping between objects in abstract (information) space (*17*–*19*). The introduction of a new computational mechanism therefore requires that we specify an input encoding, a physical mapping, and an output decoding. The specific mapping performed by the computer is referred to as the program and may be fixed by the structure of the hardware or adjusted by a separate programming mechanism.

In our SMCs, patterns of conducting and insulating fluids encode the input. As the fluid progresses, the information in the spatial pattern of the input is mapped to an electrical current by the CFRs. This output current can be used to control a variety of soft materials, actuators, or even complete robots. The mapping (i.e., the program) from input to output is controlled by the length, offset, and spacing of the CFR's electrodes, allowing the designer to program a wide range of input-output mappings. These structures operate at low voltages and pressures, do not require complex fabrication processes, and can be easily interfaced with soft mechanoreceptors.

In contrast to the plethora of computational mechanisms used by biological systems (*20*–*22*), computation in synthetic devices is almost entirely performed by electronic processors. Although there has been substantial research into unconventional mechanisms for computation (*23*–*25*), much of this work has been concerned with proving these alternatives are Turing complete (*26*, *27*). Where practical demonstrations of such approaches have been developed, they often require the use of conventional electronic computers (*28*), complex mechanisms for encoding a specific input (*29*), or cannot be easily (re)programmed (*30*).

Without practical means of integrating computation into smart materials, research has mostly been limited to engineering stimuli-response relationships (*31*–*33*). Constructing higher-level behaviors—such as decision-making, adaptation, and learning—from purely reactive mechanisms is notoriously difficult (*34*, *35*). Hence, smart

[1]Department of Engineering Mathematics, University of Bristol, UK. [2]SoftLab, Bristol Robotics Laboratory, Bristol, UK. [3]FARSCOPE Centre for Doctoral Training, Bristol Robotics Laboratory, Bristol, UK. [4]Department of Mechanical Engineering, University of Bristol, Bristol, UK.
*These authors contributed equally to this work.
†Corresponding author. Email: jonathan.rossiter@bristol.ac.uk

materials have yet to demonstrate the diversity of behaviors seen in biological materials (*36*–*38*). As a further consequence, most of the soft robots still use control approaches developed for rigid systems (*39*–*41*), introducing rigid elements (or tethers) into otherwise soft systems and therefore limiting their adaptability. The development of soft matter computing will enable roboticists to create a new class of entirely soft robots. In turn, these smart material–based robots will enable new possibilities in environmental monitoring, pollution cleanup, energy harvesting, drug delivery, wearable biosensing and prosthetic devices, and self-healing composites.

As a result, there is considerable interest in developing soft matter structures capable of providing the computation necessary for control of soft robots. For example, the microfluidics community has demonstrated analogs of many electronic components, including digital logic gates (*42*–*44*), and composed these to form integrated fluidic processing units (*45*). These devices can be fabricated using elastomeric material, composed into control systems, and integrated into soft robots (*46*–*48*). However, it is not easy to interface microfluidic controllers with nonfluidic soft actuators, and even fluidic actuation is limited by the low flow rates characteristic of microfluidic systems. Alongside being directly used to control a soft robot, SMCs can complement these approaches by interfacing microfluidic control circuits with nonfluidic soft actuators (*49*).

The SMCs use conductive fluid to transduce a fluidic signal into an electrical output. The use of conductive fluids in microfluidic circuits has previously been demonstrated in (*50*). This architecture can produce all 16 logic gates but suffers from high resistance (order of 10 megohms) and the use of DC voltages. The SMCs differ by using conduction perpendicular to the direction of fluid flow (enabling analog computation), low resistance (order of 10 ohms), and AC. Together, these make the SMCs suitable for directly powering soft actuators without the need for additional amplification or control electronics.

On a larger scale, both fluidic and mechanical switches suitable for controlling soft robotics have been developed. For example, Rothemund *et al.* (*51*) developed a soft valve capable of controlling a gripper and earthworm-like walking robot, and in (*52*), these were composed to form elementary electronic components, including two-bit adders, shift registers, and edge detectors. Fluidic controls have also been integrated into origami structures (*53*), and mechanical logic gates (*54*) can be directly 3D printed into the body of the robot. In all cases, integrating the control structure into the body of the robot was challenging. We demonstrate in this paper that SMCs can be integrated directly into the body of a robot with only minimal modification.

Another approach to embedding soft matter computation uses dielectric elastomer (DE) switches, logic devices, and oscillator circuits (*55*–*57*). These devices have been composed to create flip-flops and used to control artificial muscles (*58*). However, DEs require additional electronics to generate the high voltages necessary for their operation, and the use of thin sheets of elastomer means that they are often not robust.

Last, many soft systems have been designed to exploit the complex, passive dynamics of the body, often referred to as morphological computation (*59*). In morphological computation, the mechanical structure is designed such that the desired behavior emerges from the interaction of the robot with its environment. This can reduce—or even eliminate—the need for external control (*60*–*67*). However, although a simplification of the control problem can be identified in these examples, there is still no clear set of design principles that can be followed to exploit this effect.

Our approach is to design a fundamentally new computational mechanism using only soft materials. By developing soft computational mechanisms, we can achieve a closer integration of material and computational substrates, enabling soft robots to retain all of the benefits of soft materials and taking steps toward the intelligent, adaptive materials seen in natural systems. Figure 1A presents our concept for such a soft robotic system. Although this level of integration is not yet possible, we demonstrate the fundamental components (Fig. 1, B to D) that could be combined with developments in energy storage (*68*) and soft sensing to create such a robot. The SMC is the

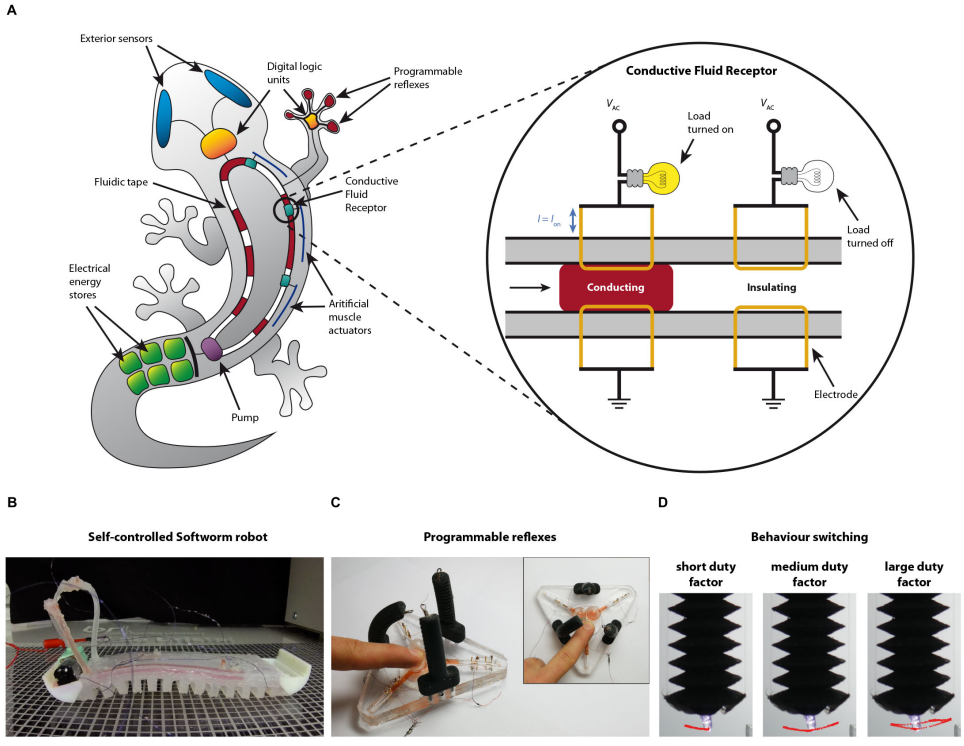

Fig. 1. The SMC. (**A**) A concept for an entirely soft, entirely autonomous robot with integrated SMC control (left). This paper demonstrates a number of the individual components necessary for such a robot. The building block of the SMC is the CFR (right). Two electrodes are connected in series with an electrical load. When conductive fluid is injected into the region between these electrodes, the load is switched on. (**B**) An SMC-controlled Softworm robot, capable of producing three behaviors. (**C**) A soft gripper with programmable reflexes provided by an integrated SMC controller. (**D**) A two–degree of freedom bending actuator that can be switched between three behaviors (i.e., tip trajectories) by varying a single parameter of the input.

mechanism that enables all of these components, and we believe that it is an important step toward the kind of integrated, autonomous, soft robot shown in Fig. 1A.

Here, we first introduce the concept behind the SMC before demonstrating a range of fundamental computational functions, including switching, amplification, filtering, and digital logic. We then demonstrate the ease with which these structures can be integrated into and used to control, soft robotic systems in three applications: (i) a Softworm robot that is controlled by an SMC that generates the control signals necessary for three distinct gaits, (ii) a soft gripper with programmable reflexes that we use to encode the sequence of actuation necessary to autonomously produce a power grip, and (iii) a two–degree of freedom bending actuator that we switch between three distinct behaviors by varying only one input parameter. We believe that our SMC is an important step toward easy-to-fabricate, untethered, and intelligent soft materials and robots.

RESULTS

The soft matter computer

The fundamental building block of the SMC is the CFR. A CFR consists of any (soft matter) tube with two electrodes placed in parallel to the direction of fluid flow but on opposing sides of the tube (see Fig. 2A for a schematic diagram). The electrodes may be completely in line with each other, overlapping, or separated by an offset. The electrodes can be connected by introducing a conductive fluid into the region of the tube spanned by the electrodes. By injecting a pattern of insulating and conducting fluids into the tube, a binary control signal is generated. As this signal progresses through the tube, any electrical load in series with the CFR is switched.

A minimal SMC consists of a single CFR, a mechanism for creating and advancing the input (the pattern of conducting and insulating fluids), and an electrical load (e.g., an actuator) to indicate the output. Input patterns may be generated during operation of the system by a controller or preloaded into the tube and advanced when triggered. When operated in this second mode, the input may be advanced by mechanical pressure generation, a DC motor–powered pump, or by using the output of another CFR to drive a low–boiling point fluid–powered soft pump. More complex SMCs can be constructed by connecting multiple CFRs together, either fluidically (by placing multiple CFRs on a single tube); electrically (by connecting the outputs of multiple CFRs together, either in series or parallel); or electrofluidically, by connecting the electrical output of one CFR to the fluidic input of another via a connection element (introduced later in this paper).

In computational terms, we consider the choice of electrode length, $L_{electrode}$; electrode offset, L_{offset}; and separation between consecutive CFRs, S, to be the program of a particular SMC. The pattern of conducting and insulating fluids represents the input to the SMC, with the output given by the current flowing through the electrical load(s).

Although independent of the choice of immiscible fluids, in this paper, we used saturated saltwater (red liquid in figures) as the conductive fluid and air as the insulating fluid. When a CFR was powered with an AC electrical signal (with a root mean square voltage V_{AC}), this led to an average on resistance of 10 ohms (and corresponding on current, I_{ON}) and an off resistance of more than 10 megohms. The on resistance is sufficiently low that many commonly used soft actuators can be driven at low voltages (5 to 15 V) via a CFR. We demonstrate this by using a CFR to control a pair of reverse polarity light-emitting diodes (fig. S1A and movie S1) and to switch both a shape-memory alloy (SMA) actuator (fig. S1B) and a low–boiling point fluid pouch motor (fig. S1C). These results show that the CFR is suitable for the control of a wide range of soft robotic systems (*69*–*73*).

Analog computing

Next, we show that a single CFR can perform analog-style computation by modifying a continuous quantity, the duty factor of the output signal, D_{out}. We further show that this modification of the duty factor can be used to allow only signals within a specific region of input parameter space to produce pulse-width modulated (PWM) outputs, with the remaining signals either fully amplified (i.e., output duty factor is 1) or fully filtered (i.e., output duty factor is 0). Within this region, input signals are modified according to the sign and magnitude of the effective electrode length, L_{eff}.

In digital systems, PWM signals are commonly used to represent analog quantities such as voltage. PWM signals are described by a frequency and a duty factor (which represents the fraction of the waveform that is high), with the duty factor used to represent the analog quantity. For example, if our system had a minimum voltage of 0 V and maximum voltage of 5 V, then we would map 0 V to a PWM signal with duty factor of 0, 2.5 V to a duty factor of 0.5, and 5 V to a duty factor of 1.

We considered PWM input signals—characterized by a wavelength, λ, and input duty factor, D_{in}—that represent the fraction of the input signal that is conductive (see Fig. 2A, top). Although PWM signals are typically described in terms of frequency, wavelength is the natural representation for our spatial input signals. Note that frequency domain versions of the plots in this section are also available in fig. S4. We assumed a constant flow rate for the input and began our analysis once the tape progressed an initial distance L_0 such that the left edge of the first conductive region was in contact with the start of the first electrode. We also introduced the defining parameter of the CFR geometry, the effective electrode length, $L_{eff} = L_{electrode} - L_{offset}$. This is the extent to which the two CFR electrodes overlap. A negative L_{eff} corresponds to the case where the distance between the two electrodes, L_{offset}, is greater than the electrode length, $L_{electrode}$.

When passing through a CFR, a pulse of conductive fluid of length $L_{conductive} = \lambda D_{in}$ will cause an output pulse of length $L_{conductive} + L_{eff}$ (see Fig. 2A for a pictorial representation of the mechanism, for cases where $L_{eff} = L_{electrode}$ and $L_{eff} < 0$) and output duty factor $D_{out} = D_{in} + L_{eff}/\lambda$. This means that the sign of L_{eff} can be used to determine whether the CFR acts as an amplifier (by increasing the duty factor, D_{out}, and thus power of the output) or filter (by decreasing the duty factor, D_{out}). The magnitude of L_{eff} determines the amount of amplification or filtering. We explored this further by considering two cases: fixed wavelength and fixed input duty factor.

Fixed wavelength

Figure 2B plots the output duty factor for two fixed wavelengths [λ = 100 mm (top) and λ = 25 mm (bottom)] against input duty factor, for a range of values of L_{eff}. In the case of positive L_{eff}, low duty factor input signals produce PWM output signals, whereas inputs with duty factor above the cutoff value of $D_{cutoff} = 1 - (L_{eff}/\lambda)$ produce an output that is constantly on. If L_{eff} is negative, then the high duty factor input signals will produce an output, but those with an input duty factor below $D_{cutoff} = L_{eff}/\lambda$ will not. Thus, if the input

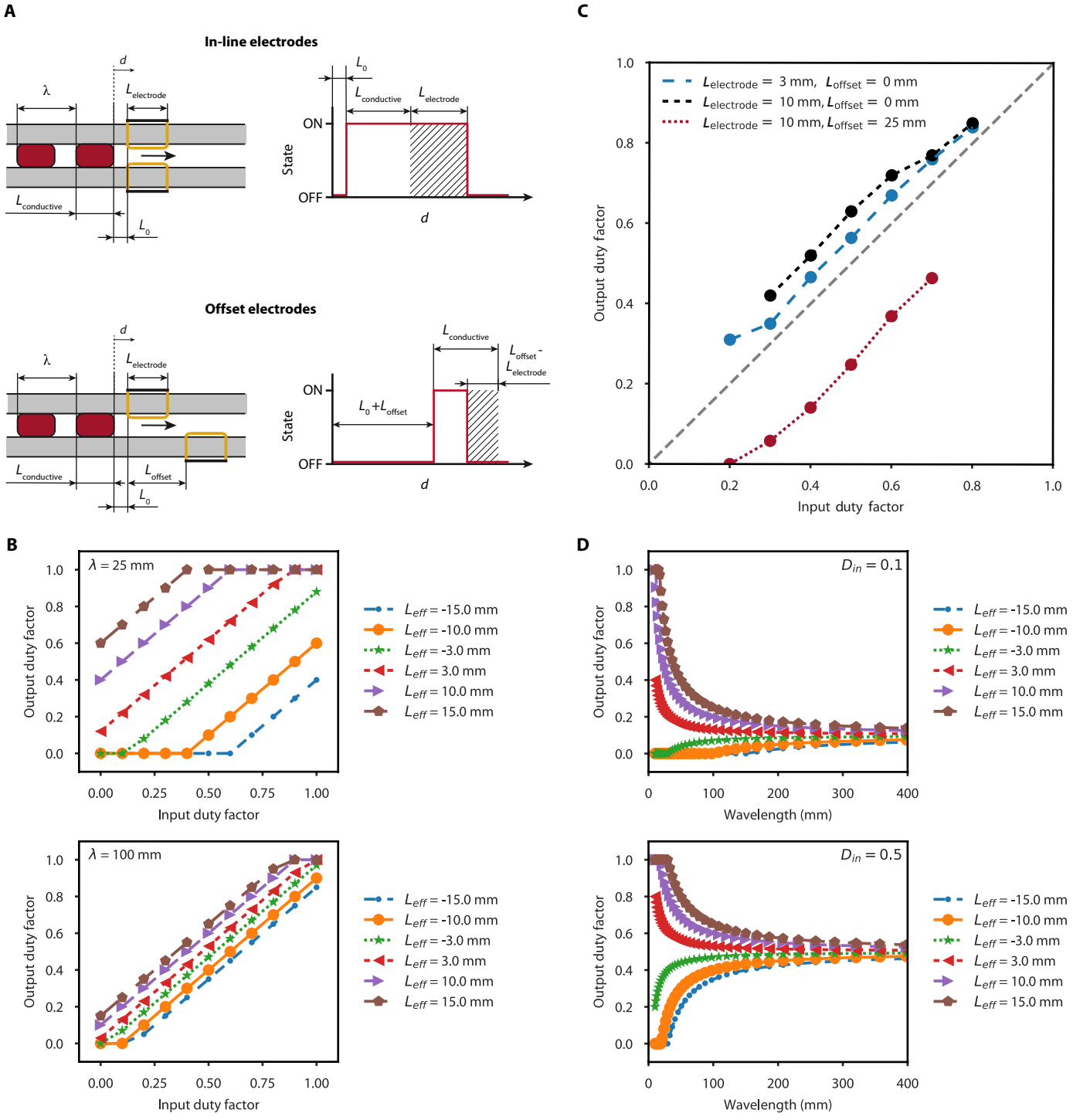

Fig. 2. Analog soft matter computing. (**A**) The mechanisms by which the inline (top) and offset (bottom) versions of the CFR can filter or amplify, respectively, the duty factor of PWM input signals. The right-hand images show the idealized output of each CFR, with the effect of the CFR geometry on the input signal (wavelength λ, conductive region length $L_{conductive} = \lambda D_{in}$) shown in the shaded region. (**B**) The relationship between D_{in} and D_{out} for fixed λ = 25 mm (top) and λ = 100 mm (bottom). (**C**) The output duty factor is plotted against input duty factor for three CFR geometries, an input of λ = 100 mm, and D_{in} values ranging from 0.2 to 0.8. (**D**) The relationships between input λ and D_{out} for $D_{in} = 0.1$ (top) and $D_{in} = 0.5$ (bottom).

wavelength is fixed, by selecting L_{eff}, a designer can determine whether a CFR allows high or low duty factor signals to produce PWM outputs and the cutoff value where this occurs. For example, if we create a CFR with $L_{eff} = -15$ mm and apply an input signal of λ = 100 mm, then only inputs with $D_{in} > D_{cutoff} = 0.15$ will result in a nonzero output. On the other hand, if $L_{eff} = 10$ mm, then only inputs with $D_{in} < D_{cutoff} = 0.9$ will produce a PWM output.

We confirmed these relationships by applying input signals of λ = 100 mm and duty factors ranging from 0.2 to 0.8 to test CFRs with L_{eff} of 3, 10, and −15 mm. Figure 2C plots the corresponding duty factors. The relationship is shown to hold, with L_{eff} = 3 mm mapping to outputs slightly above the line of unity mapping (the response when input is mapped to output without change), whereas L_{eff} = 10 mm is further above this. As expected, L_{eff} = −15 mm maps to an output below the unity line. Note that although the high-pass filtering effect of the offset CFR was confirmed, at the highest duty factors, the signal through the in-line CFR began to break apart (see fig. S5 for further information on this effect).

Fixed duty factor

Figure 2D plots the output duty factor for the case where the input duty factor is fixed [D_{in} = 0.1 (top) and D_{in} = 0.5 (bottom)], and the wavelength is varied for the same values of L_{eff} used above. In both cases, large wavelength (i.e., low frequency) signals could pass with only minimal modification. For small wavelength signals, the output duty factor was modified, with the effect determined by the sign of L_{eff}. In the case of positive L_{eff}, low wavelength signals were amplified, with the cutoff wavelength given by $\lambda_{cutoff} = L_{eff}/(1 - D_{in})$, whereas in the case of negative L_{eff}, low wavelength signals were filtered, with the cutoff wavelength given by $\lambda_{cutoff} = L_{eff}/D_{in}$. For example, if we have a CFR with L_{eff} = 10 mm and D_{in} = 0.5, then signals with $\lambda < \lambda_{cutoff}$ = 20 mm will be fully amplified (i.e., $D_{out} = 1$). Figure S4 plots the same data as Fig. 2D in the frequency domain.

We have shown that an SMC containing only a single receptor can perform analog computation by modifying the duty factor of PWM input signals. The specific computation performed by the system can be programmed in hardware (by varying the electrode length) or in software (by changing the wavelength or input duty factor of the signal). This shows that an SMC can be programmed to differentially filter PWM input signals, allowing only some signals to produce PWM outputs, whereas others are either fully amplified or fully filtered. This ability forms the basis of a simple behavior switching system, demonstrated later in this paper.

Digital computation

Alongside the analog computation, it is also straightforward to conduct digital computation by electrically connecting multiple CFRs. By connecting two CFRs either in parallel or series and varying whether the CFRs are initially connected by conducting fluid, we could construct all fundamental binary operators, except for XOR. Note that XOR can be easily constructed by composing multiple SMC gates. Figure 3A shows the schematics of five possible configurations. To confirm these gates function as expected, we fabricated each and used them to drive an SMA actuator to visually indicate the output. Figure 3B shows the NOT gate, superimposed on the current through the CFR, and Fig. 3C demonstrates the remaining logic gates. Movies S2 to S5 show the

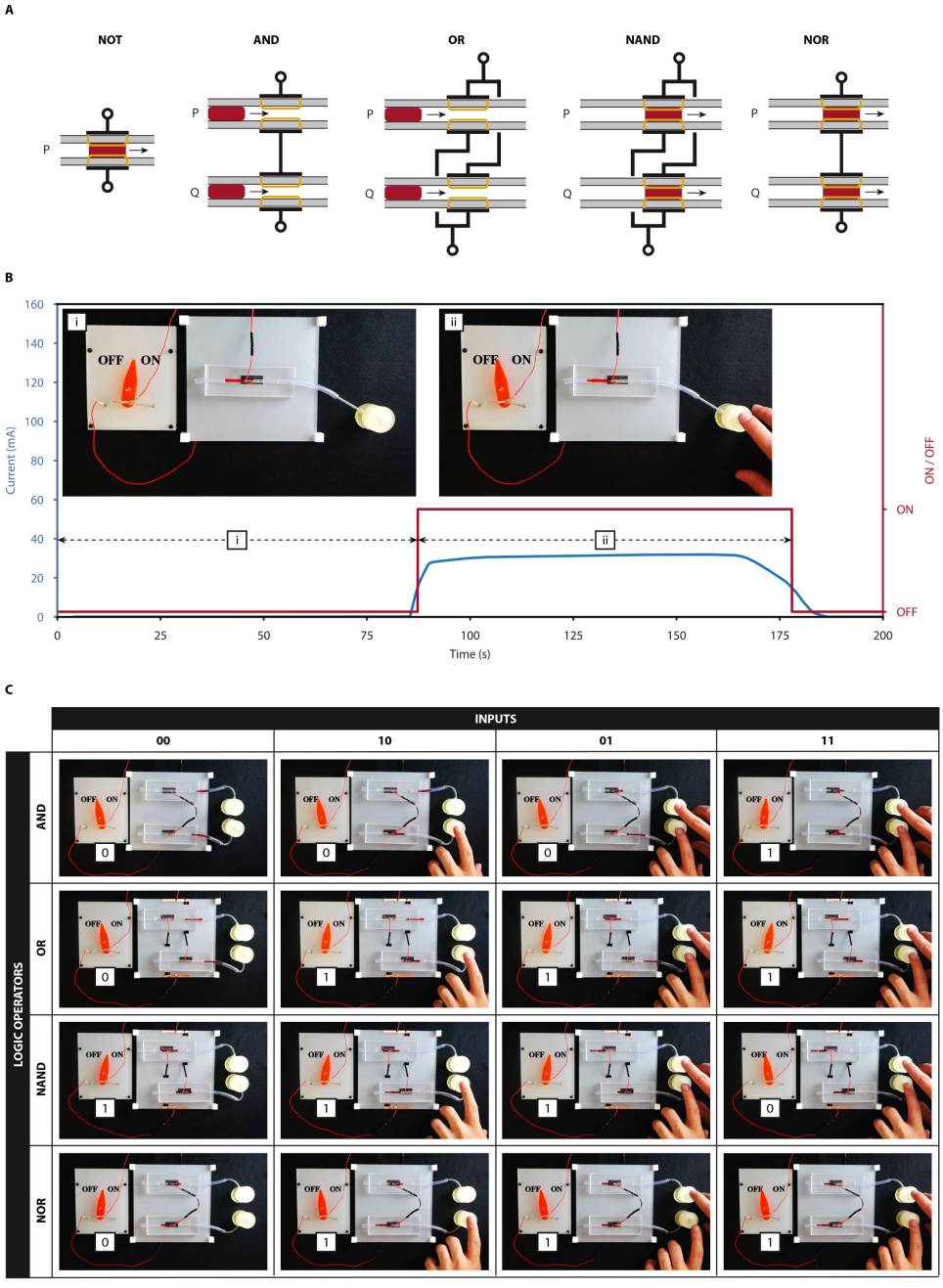

Fig. 3. CFR logic elements. (**A**) By connecting two CFRs either in parallel or serial, all fundamental logic elements bar XOR can be built. (**B**) A NOT gate is used to drive an SMA actuator. (**C**) The full truth tables are demonstrated for the remaining logic elements.

AND, OR, NAND, and NOR configurations, respectively, driving the SMA output indicator. In all cases, the expected truth table output is demonstrated. Note that because of the serial and parallel addition of the respective resistances, an output driven by an AND gate will see an SMC resistance of about 20 ohms, whereas an output driven by an OR gate will see a resistance of 5 ohms.

To create more complex functions, it is necessary to compose multiple logic gates. To do this with the SMC, we developed an electrofluidic diode (ED) that sends the output of one CFR to the input of another. The ED was formed by sealing a conductive fabric heating element and a small amount of low–boiling point fluid inside a pouch motor (*74*) and then sealing this pouch motor inside a urethane vessel with a fluidic output port. The ED converts electrical input energy (and information) to mechanical output energy (pressure). The ED required about 100 mA to activate and was easily powered by the output of a CFR (*75*). We could compose two CFRs by using an ED as the electrical load connected to one CFR and attaching the fluidic output of the ED to the second. Figure 4A shows a composite SMC, and Fig. 4B shows a schematic diagram of the ED. The composite SMC consists of a (mechanical) pressure-driven switch (CFR1) and a CFR NOT gate (CFR2), joined by an ED. When the mechanical pump was activated, it advanced the fluid in the CFR1, applying current to the ED. This generated an output pressure, which advanced the fluid into CFR2. This, in turn, switched the output of CFR2 (an SMA-powered indicator) off. Movie S6 shows this sequence. This behavior is shown in Fig. 4A, which shows key frames of this sequence, and Fig. 4C, which shows the current through the two CFRs, respectively. The use of the ED to make this connection causes an additional switching time of 5 s. By miniaturizing the ED, we expect to greatly reduce both the switching delay and activation current.

The ability to compose multiple logical functions into a more complex structure enables the exploitation of the many logical and computational structures used in digital electronics. These structures could lead not only to reactive soft robots but also to systems that have a form of memory (e.g., via composing multiple gates into a flip-flop structure).

Controlling robots with SMCs

To demonstrate the potential of the SMC in robotics, we used SMCs to control three soft robots.

Self-controlled Softworm robot

First, we show that an SMC controller could be integrated directly into the body of a Softworm robot, inspired by (*76*). Figure 5A shows top and side views of the SMC-Softworm with a closed channel for the fluidic input tape and spacing for two CFRs embedded into the structure. Softworms move by exploiting the contraction of two SMA actuators embedded in their underside and the controllable friction of the two feet. By varying the contact angle of the feet, it is possible to switch between low- and high-friction states. A crawling gait can be produced by creating a pattern of actuation that switches on one SMA and then, after some time, switches on the second SMA. After further time, the first SMA is switched off, and last, the second is switched off. Figure 5B shows the desired pattern in terms of SMC activation. Further details can be found in (*76*, *77*).

To create this pattern of actuation in our SMC-Softworm, we placed the electrodes such that the spacing between electrodes [S_1 and S_2, as shown in Fig. 5 (B to D)] was not equal and injected an amount of conductive fluid with $S_2 > L_{conductive} > S_1$. The closed-loop tape was advanced by a peristaltic pump mounted on top of the

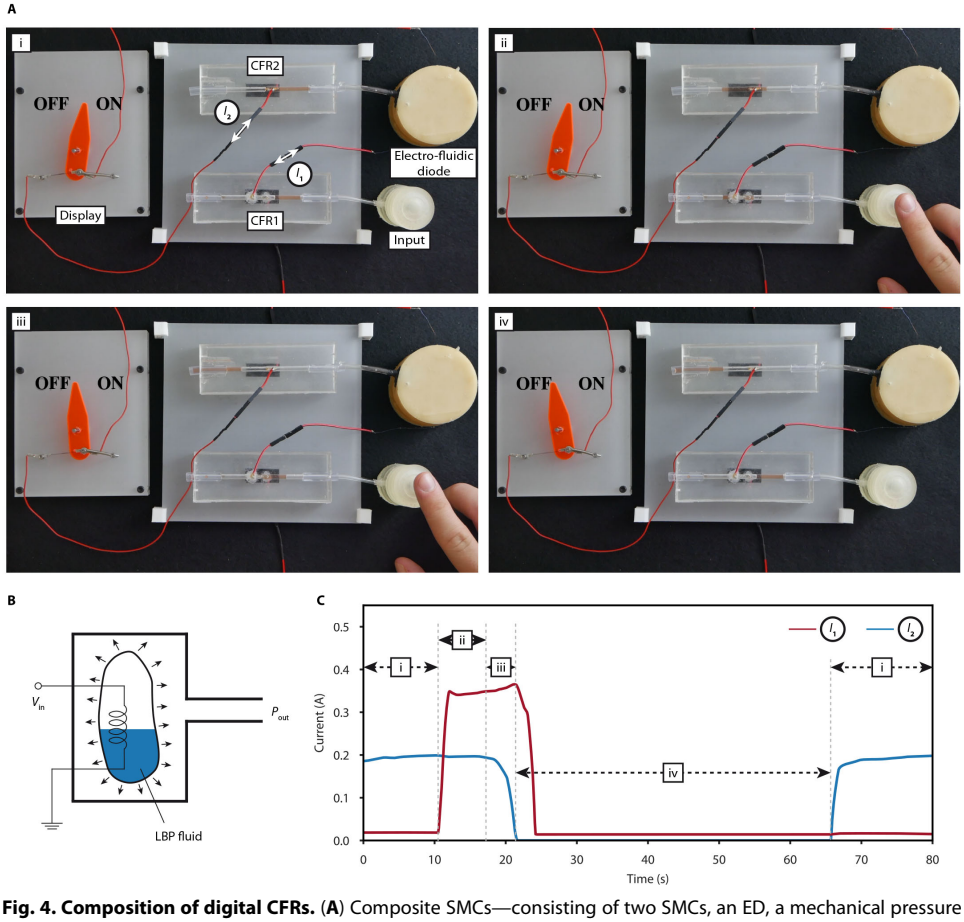

Fig. 4. Composition of digital CFRs. (**A**) Composite SMCs—consisting of two SMCs, an ED, a mechanical pressure input, and an SMA actuated display—are shown. CFR1 is in the switch configuration, has an input advanced by a mechanical pump, and has the ED as its output. CFR2 is in the NOT gate configuration, has an input advanced by the ED, and has an SMA-driven display as its output. In (i), the mechanical pump is switched off, meaning the input to CFR1 is also off. Because CFR2 is a NOT gate, this means the display is turned on. In (ii), the mechanical input is turned on, connecting CFR1 and causing current to flow. This current drives the pouch motor inside the ED. In (iii), the pressure generated by the ED has advanced the conductive fluid beyond CFR2, switching the display off. In (iv), mechanical switch is released, switching CFR1 off. The output remains off while the fluid inside the ED returns to its initial position. (**B**) A schematic of the ED. When a voltage V_{in} is applied to the conductive fabric heating element, the resultant Joule heating causes the low–boiling point (LBP) fluid to boil. This increases the pressure P_{out} at the outlet of ED. (**C**) The current through the two CFRs during this sequence.

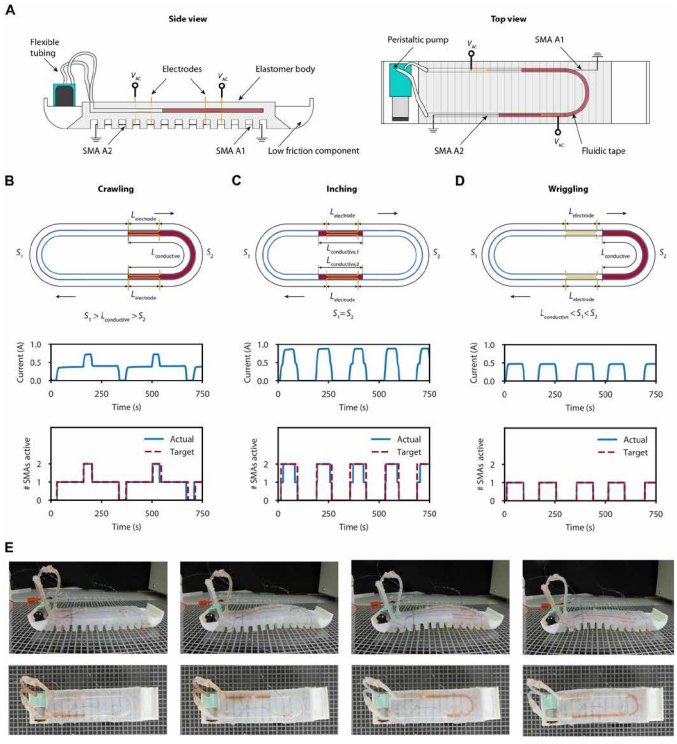

Fig. 5. A Softworm with integrated SMC controller. (**A**) A schematic diagram from both side and top views. (**B** to **D**) The input patterns required to produce crawling, inching, and wriggling gait, respectively, with the current drawn by the Softworm below. (**E**) Both top and side views of the crawling gait.

robot. Figure 5E shows key frames of the top and side views of the CFR-controlled Softworm during locomotion. The CFR-controlled worm moves at a mean forward velocity of 0.333 mm/min (see movie S4). This is lower than the original Softworm (*78*) and is due to the low speed of the onboard peristaltic pump and the limitations on the speed with which a stable signal can be propagated through a CFR. This limitation is discussed in detail later in this paper. Note that the speed of the Softworm could also be increased by reducing the length of the channel the input flows through. In this case, we chose the design that was easiest to manufacture.

Softworms have also been shown to be capable of both inching and wriggling behaviors (*78*). The control signals for these two gaits are shown in Fig. 5 (C and D, respectively). To create the inching gait, we altered the positioning of the CFRs such that the two CFRs divided the entire tube into two equal sections (i.e., $S_1 = S_2$). We also modified the input pattern to consist of two equal lengths of conductive fluid ($L_{\text{conductive},1}$ and $L_{\text{conductive},2}$), separated by two equal lengths of insulating fluid (i.e., $L_{\text{conductive},1} = L_{\text{conductive},2} < S_1 = S_2$). To create the wriggling control signal, we varied the initial pattern of (input) fluid that was injected to the Softworm. By reducing the length of the conductive region such that $L_{\text{conductive}} < S_1 < S_2$, we altered the program of the system to create a control signal that causes the first SMA to turn off before the second SMA is actuated. Figure 5 (B to D) shows the current measured through each CFR against time, demonstrating that all three possible Softworm control signals can be created with the SMC.

Simple oscillatory signals are often sufficient to generate locomotion (*79*–*81*). Typically, these are generated by a conventional microcontroller, either integrated into the system or attached via a tether. The SMC represents a facile method by which a system for generating such signals can be integrated into the body of a soft robot. Although this instantiation of the SMC still uses a rigid component (in the form of a peristaltic pump used to advance the input), eliminating the need for external control electronics represents a step toward untethered, fully soft robots.

Programmable reflexes in a soft robotic gripper

Next, we show how the digital computation performed by the SMC can be used to program the reflexes of a soft gripper. Figure 6 (A and B) shows the design of an SMC controller for three SMA-actuated fingers. Each finger was connected to two CFRs in an OR gate configuration. These two CFRs were located along the same tube and attached to a mechanical (pressure) input containing conductive fluid. When pressure was applied to an input, the conductive fluid moved through the channels into the CFR regions. The applied voltage was selected such that the current through a single CFR provides enough heating to prime the actuator but is insufficient to activate the SMA. When further pressure was applied, the second CFR was connected, causing rapid actuation of the SMA finger. Figure 6C shows the total current flowing through the gripper when all three inputs are pressed simultaneously, and Fig. 6D shows the current when each input is pressed and released sequentially. By controlling the amount of fluid injected into the input chamber, we varied the distance that the fluid had to travel through the channels before reaching the CFRs. In this way, we mechanically programmed a power grip action, in which two of the fingers perform an initial grasp, with the third actuating later. Figure 6 (E and F) shows key frames of this sequence, and movie S8 shows each finger activated in turn, followed by the simultaneous activation, causing the power grip.

There are a variety of cases where the delicate touch of a soft gripper is necessary, including sampling from coral reefs (*82*), picking fruit (*83*), and handling fragile materials (*84*). In most cases, these devices are controlled with conventional electronics via a tether. An SMC could be used alongside conventional electronics to provide a set of fast, locally controlled reflexes without requiring the integration of rigid components.

Behavior switching in a two–degree of freedom soft actuator

Last, we show that a single SMC can produce multiple behaviors by varying only a single parameter of the input signal (the duty factor in this case). To demonstrate this, we designed a two–degree of freedom bending actuator and controlled it with a single SMC containing two CFRs (see Fig. 7A). The first CFR (CFR1) had offset electrodes, with $L_{\text{electrode}} = 10$ mm and $L_{\text{offset}} = 25$ mm. The second CFR (CFR2) was in line with electrode length $L_{\text{electrode}} = 10$ mm. Note that this meant that the two CFRs had differing resistances; to drive the system at a single voltage, we used a 120-ohm resistor, R, in series with CFR2 to ensure that the current through each SMA was approximately the same. These two CFRs were separated by a distance of $S = 40$ mm. We applied an input signal with a wavelength of $\lambda = 120$ mm and varied only the duty factor. Key frames from one of these sequences are shown in Fig. 7B. With a duty factor of 0.1, the conductive region ($L_{\text{conductive}}$) had a length of 12 mm, enough to activate CFR2 but not CFR1. When applied to the bending actuator, this caused it to alternate between its resting position and one-sided bending. The trajectory generated by this input is shown in Fig. 7C. Increasing the duty factor to 0.5 generated an input signal with $L_{\text{conductive}} = 60$ mm. This switched CFR1 on and then off, before activating CFR2. This caused

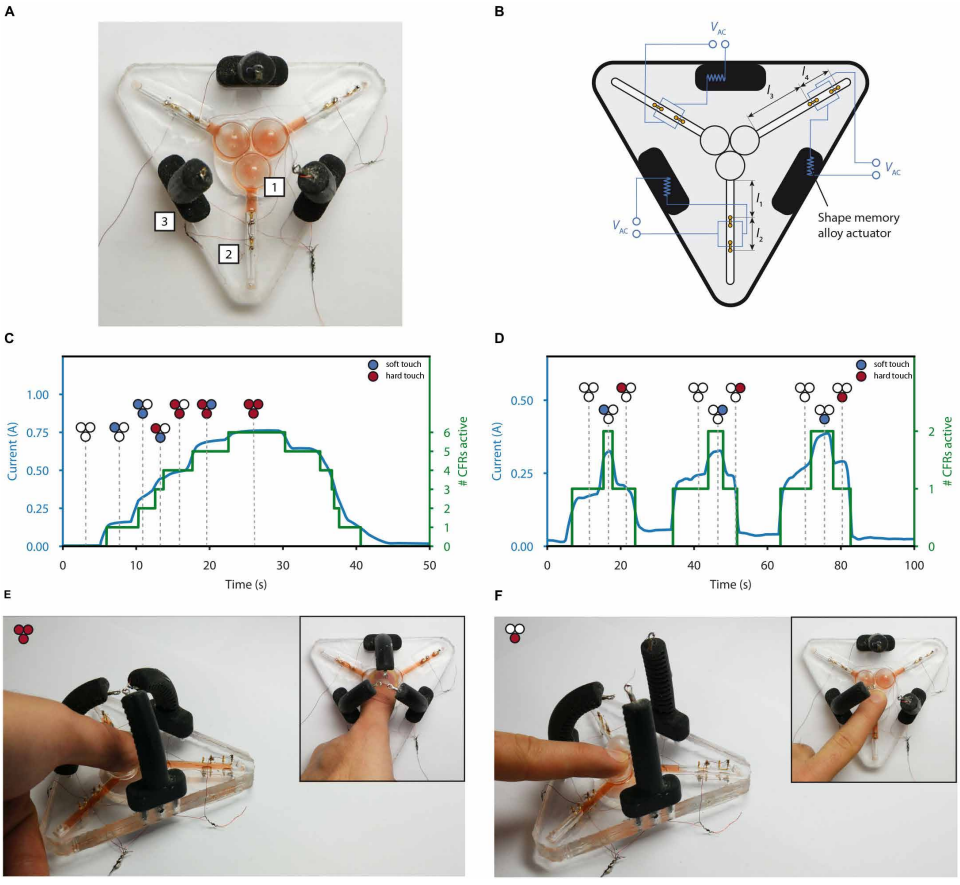

Fig. 6. Programmable reflex gripper. (**A**) A top view and (**B**) a schematic diagram of the gripper. (**C**) The current through the gripper during pressing of all three inputs (simultaneously). (**D**) The current through the gripper for a sequence of three individual presses, stimulating a different finger for each of the presses. (**E**) The top and side views of the fully actuated gripper. (**F**) The top and side views when the bottom pressure input is pressed and the left finger actuating in response.

the actuator to switch between the two opposite bending states, via the resting state. This trajectory is shown in Fig. 7D. Last, we applied a signal with a duty factor of 0.8. This caused the CFR2 to activate before CFR1 switched off. When applied to the actuator, this generated a 2D cyclic path for the end of the actuator, as shown in Fig. 7E. During this sequence, the tip moved via a compressed state caused by the simultaneous activation of both SMAs. These cycles can be seen in movie S9.

By simply changing the fluid input control sequence, we were able to selectively transition between a range of actuation trajectories. Specifically, we used a change in a continuous quantity, the length $L_{\text{conductive}}$ of the conductive region, and therefore the duty factor D_{in} to switch between distinct behaviors. Using change in a continuous quantity to switch between qualitatively different behaviors has been proposed to explain the switch between swimming and walking in salamanders (*85*) and a range of other behaviors (*86*). These results suggest that an SMC not only can generate oscillatory or reflexive signals but also can be used to control robots where switching between behaviors is needed.

DISCUSSION

This paper presents the SMC, a soft-matter computational mechanism that can be easily integrated into soft robots. An SMC consists of one or more CFRs, representing the program of the SMC, and a pattern of conducting and insulating fluids as input. We have shown that even a single CFR is sufficient for performing analog computations and that digital computation is possible with two or more CFRs. We have also shown that it is possible to compose SMCs in a variety of ways, meaning the space of possible SMC architectures is far larger than those presented in this paper.

A natural question to consider when introducing a new computational mechanism is the range of mappings it can perform. It has been shown that the composition of electronic logic gates can compute any function from the wide class of general recursive functions (*87*). The SMC can implement the same binary operations performed by these gates, meaning that theoretically, it can be a basis for a Turing complete computational mechanism. Although there are still fabrication challenges to be overcome before large-scale integrated SMC structures are feasible, there are many use cases where the minimal computation demonstrated here is sufficient. We believe that the SMC is particularly suited for providing local, reflexive control for soft grippers and for generating oscillatory control signals for locomotion, without the need for conventional electronics (*88*).

Furthermore, for certain computations, we expect that an SMC architecture is a more natural fit than a traditional electronic microcontroller. The CFR represents a fundamentally different mechanism to that used by digital logic gates, with the ability to easily mix analog- and digital-style computations and with a natural representation of a pulse of information. For example, although we can simulate spiking neural networks using conventional electronics, this requires the integration of the differential equations describing the dynamics of the neuron. The SMC, on the other hand, could naturally represent the notion of a spike with a short length of conductive fluid.

We have also shown that it is possible to integrate the SMC directly into the body of a number of soft robots. This requires only the addition of a channel for the tape to flow through, the attachment of the electrodes, a suitable mechanism for advancing the tape, and an AC signal source—all of which can be easily placed on board the system. In all three demonstrations, we have used an SMA actuator as the output of the SMC. However, it is possible to use the output of an SMC to control any electrically or thermally driven actuator, making them suitable for controlling a wide range of robots. Furthermore, as the SMC transduces a fluidic input into an electrical output, it is also capable of interfacing more technologically mature microfluidic control circuits with nonfluidic soft actuators (*49*). This vastly increases the design space for such systems and enables the use of fast and/or high-power soft actuators, such as SMAs, ionic-polymer metal composites, and pouch motors.

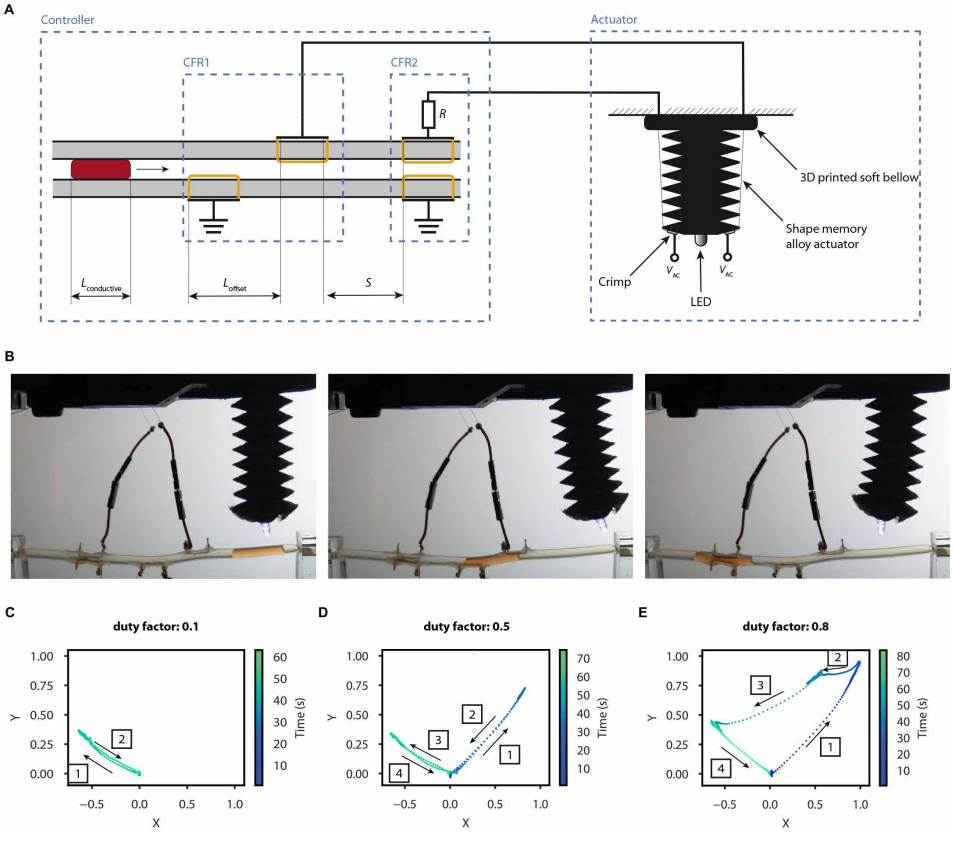

Fig. 7. Behavior switching by varying a single input variable. (**A**) Schematic diagrams of both the SMC and the two–degree of freedom bending actuator. Briefly, the SMC consists of two CFRs separated by a distance $S = 40$ mm. Both CFRs have $L_{electrode} = 10$ mm. CFR1 has $L_{offset} = 25$ mm, whereas CFR2 has $L_{offset} = 0$ mm. A resistance of $R = 120$ ohms is placed in series with CFR2. (**B**) Three key frames from the behavior produced when driven with an input signal with a duty factor of 0.5. (**C**) Tip trajectory when the SMC is given an input with a short (0.1) duty factor. (**D**) The tip trajectory when the SMC is given an input with a medium (0.5) duty factor. (**E**) The tip trajectory when the SMC is given an input with a large (0.8) duty factor. In (C) to (E), both *X* and *Y* are normalized dimensions.

For an SMC-controlled robot to operate completely untethered and not require any rigid components, it is necessary to develop soft mechanisms for creating an input, advancing the input, and generating an AC signal. In the simplest case, input patterns can be generated before operation, stored in a section of tube, and only advanced during operation (equivalent to programming a microcontroller with an external programmer). Digital SMC architectures can be used to switch between multiple preloaded tapes to create more complex behaviors. An entirely soft tape generation mechanism could be created by composing multiple SMCs into a flip-flop structure and using this to control two ED-based pumps. These ED-based pumps would require the addition of an extra outlet and a check valve on each outlet to function correctly. For advancing the tape, we have demonstrated two soft mechanisms: a mechanical bellow and the ED. However, there are many alternative soft pressure sources (*89*–*91*), such as the catalyzed decomposition of hydrogen peroxide, that are also suitable for autonomously advancing the input. On the other hand, generating an AC signal without rigid components is challenging, and we are currently investigating a range of alternative conductive fluids, such as liquid metals, to eliminate the need for an AC signal.

We are also considering alternative computational mechanisms inspired by the way information is encoded in the SMC. In the SMC, electrodes create a response when they are bridged by a conductive fluid; the mutual conductivity of the electrodes and fluid transduces the information in the fluidic input into an electrical response. However, this principle of encoding information in the spatial structure of a fluid is independent of any specific transduction mechanism. For example, we could replace the electrodes with catalysts (e.g., platinum), triggering a response when the correct mixture of reactants (e.g., H_2O_2) flow into the active (catalyzed) region.

Throughout the development of these devices, we encountered two main limitations. First, even at high frequencies, a single CFR has a resistance of about 10 ohms, limiting the amount of current we can deliver. Combining units in series compounds this problem, as does adding an offset to the electrodes. Although this can be overcome by the construction of an electronic buffer circuit, this comes at the expense of added complexity. We expect that alternative conductive fluids such as liquid metals will overcome this limitation. Second, determinism in the SMC requires that the lengths of the conductive and nonconductive fluid regions remain approximately constant throughout operation. We tested the long-term stability of the SMC pattern, finding that at low speeds, the pattern was stable, with a mean duty factor changing from 0.174 to 0.151 after 8 hours of operation (see fig. S6). We suspect that much of this variation may be due to imperfect sealing of the tube. However, we found that the pattern can be affected if the fluid is advanced too quickly. This is due to a viscous boundary layer that forms between the saltwater and the tube. At low flow rates, this viscous layer remains attached to the rest of the fluid and progresses with it. At higher speeds, this layer detaches from the fluid, to be then collected by the next section of saltwater. Last, at high enough speeds, the depth of the viscous boundary layer is enough to connect two conductive regions. At this point, fluid does not flow along the tube in discrete elements anymore (see fig. S5 for images of the salt water tape breaking down). Movie S10 demonstrates an SMC actuating an SMA actuator at the maximum currently attainable speed. We also found that the use of AC current means that no observable electrolysis occurs during operation (see fig. S7 for a comparison of the observable electrolysis for AC and DC voltages).

Conversely, we found that the tape remained intact during body deformation. This is best observed in the SMC-Softworm, where large deformations of the body were necessary for locomotion, yet the tape remained intact throughout. We repeated the long-term stability test with a deformed tube and found that the mean duty factor reduced from 0.23 to 0.175 after 8 hours of operation (see fig. S6B). We expect that extreme deformations (enough to cause buckling

within the tube) or deformation that is localized to the CFR region would, however, affect the operation of the SMC.

The interplay between the various forces affecting the tape as it progresses through the SMC also determines the length scales where the SMC concept could be applicable. The Reynolds number for flow in a tube scales linearly with the mean velocity of the fluid and the hydraulic diameter of the tube, meaning that as the SMC is miniaturized, higher fluid velocities become possible without inertial effects influencing the flow. Similarly, the balance of viscous forces to interfacial tension is captured by the dimensionless capillary number, Ca, which is linearly proportional to fluid velocity. This suggests that the SMC concept should be applicable at the microscale, and we are currently exploring microfluidic fabrication techniques to realize this.

This paper has presented the SMC, a soft matter computational mechanism that can be easily integrated into soft robots and used to control a wide range of soft robots. The mechanism uses the placement of electrodes to control the way in which an input pattern of conducting and insulating fluids is mapped to an output current flowing through the electrodes. The mechanism can be used to create analog, digital, or hybrid computations and can be easily integrated into smart materials or soft matter robots, paving the way for more sophisticated soft robots and intelligent compliant structures.

MATERIALS AND METHODS

Fabrication of a CFR

CFRs were made from polydimethylsiloxane (PDMS; Farnell, UK). Molds for the two halves of a CFR were first printed on an Objet Connex in VeroWhite. PDMS parts A and B were mixed in a 10:1 ratio, poured into the mold, and cured for 24 hours at 40°C. Once cured, gold-plated copper wire electrodes were cut to length, bent to shape by hand, and inserted into the CFR halves. The two halves were then sealed together with a layer of uncured PDMS, and silicone tubing was sealed into both ends, also with a layer of uncured PDMS. We were also able to fabricate working CFRs by hand sewing electrodes into prefabricated silicone tubes.

Frequency response and resistance measurements

The frequency response of a CFR was measured with a potential divider setup. A potentiostat (Hokuto Denko HA-151B) was used to provide the input voltages, with resistance calculated by measuring the voltage drop across a 10-ohm load resistor (RS Components, UK) with a data acquisition unit (NI-USB 6229, National Instruments, UK). A similar approach was used to measure the resistance when investigating the relationship between electrode offset and resistance. This setup was also used for the reliability tests. In this case, the input was advanced by the same peristaltic pump used to power the Softworm robot. The pump was operated continuously for 8 hours, with current measurements taken for 10 min at hourly intervals. A Python script was used to calculate the duty cycle throughout this period.

Fabrication of pouch motors

Pouch motors were fabricated from polyethylene. A total of 40-mm lengths of polyethylene tube were cut and heat-sealed along one edge. Wires were hand sewn into a conductive fabric (Adafruit Knit Jersey Conductive Fabric, Farnell, UK) that formed a heating element, and this was placed into the half-sealed polyethylene. One milliliter of low–boiling point fluid (Novec 7100, Sigma-Aldrich, UK) was injected into the bag. Last, the top of the bag was also heat-sealed.

Fabrication of ED

The ED was made from VytaFlex 30 (Bentley Advanced Materials, UK). Molds were printed on the Objet Connex out of TangoBlack. VytaFlex parts A and B were mixed in a 1:1 ratio, degassed, poured into the mold, and left to cure for 4 hours at 40°C. Separately, a lid for the chamber was cast. The pouch motor was placed inside the chamber, and the connecting membrane was then sealed on top of the chamber with uncured VytaFlex 30. Once cured, an outlet hole was cut and a silicone tube was sealed with further VytaFlex 30.

Fabrication of the Softworm robot

Molds for the top and bottom parts of the Softworm were printed on an Objet Connex out of VeroWhite. Separately, the low friction feet of the worm were also printed in VeroWhite. The Softworm was cast out of SORTA-Clear 12 (Bentley Advanced Materials, UK). Parts A and B were mixed in a 1:1 ratio, degassed, and poured into the mold. After curing for 4 hours at 40°C, gold-plated copper electrodes were cut, shaped by hand, and placed into the appropriate locations. The two halves were then sealed together with a layer of uncured elastomer. The two feet were also attached with a layer of uncured elastomer. Last, SMA actuators were cut to length and threaded through the body of the Softworm. Two short lengths of silicone tubing were attached to each end of the fluid channel and attached to a micro–peristaltic pump (RP-Q1 Miniature Peristaltic Pump, Takasago Electric).

Fabrication of the gripper

Molds for the gripper base were printed in VeroWhite on an Objet Connex. PDMS elastomer was mixed in a 10:1 ratio, poured into the molds, and allowed to cure for 24 hours at 40°C. Once cured, electrodes were cut to length, bent to shape, and placed by hand. The two halves were then sealed together with a further layer of uncured elastomer. Separately, a two-part mold for the input domes was printed on the Objet Connex (top part, VeroWhite; lower part, TangoBlack). PDMS was mixed as before and poured into the lower mold. The upper mold was then pressed into the lower mold. Once cured, the domes were sealed on top of the gripper with a further layer of uncured PDMS. Three fingers were printed on an Objet Connex in TangoBlack. SMA actuators were threaded into the channels shown in Fig. 6. The fingers were bonded into the gripper using Sil-Poxy. Last, a mixture of salt, water, and red food dye was mixed and injected into the input chambers.

SUPPLEMENTARY MATERIALS

robotics.sciencemag.org/cgi/content/full/4/33/eaaw6060/DC1

Fig. S1. Three outputs controlled by SMCs.
Fig. S2. Frequency response of the CFR at three voltages.
Fig. S3. Resistance through a CFR as electrode offset is varied for three voltages.
Fig. S4. Frequency domain analog computing results.
Fig. S5. Stability of the fluidic tape.
Fig. S6. Long-duration actuation test.
Fig. S7. Electrolysis demonstration.
Movie S1. CFR concept.
Movie S2. CFR AND gate.
Movie S3. CFR OR gate.
Movie S4. CFR NAND gate.
Movie S5. CFR NOR gate.
Movie S6. Composite SMC.

Movie S7. SMC Softworm.
Movie S8. SMC gripper.
Movie S9. SMC behavior switching.
Movie S10. Fast actuation demonstration.

REFERENCES AND NOTES

1. S. Kim, C. Laschi, B. Trimmer, Soft robotics: A bioinspired evolution in robotics. *Trends Biotechnol.* **31**, 287–294 (2013).
2. C. Laschi, B. Mazzolai, M. Cianchetti, Soft robotics: Technologies and systems pushing the boundaries of robot abilities. *Sci. Robot.* **1**, eaah3690 (2016).
3. C. Majidi, Soft robotics: A perspective-current trends and prospects for the future. *Soft Robot.* **1**, 5–11 (2014).
4. M. Taghavi, T. Helps, B. Huang, J. Rossiter, 3D-printed ready-to use variable-stiffness structures. *IEEE Robot. Autom. Lett.* **3**, 2402–2407 (2018).
5. M. Cianchetti, Fundamentals on the use of shape memory alloys in soft robotics. *Interdisc. Mechatron. Eng. Sci. Res. Dev.*, 227–254 (2013).
6. C. S. Haines, M. D. Lima, N. Li, G. M. Spinks, J. Foroughi, J. D. W. Madden, S. H. Kim, S. Fang, M. J. de Andrade, F. Göktepe, Ö. Göktepe, S. M. Mirvakili, S. Naficy, X. Lepró, J. Oh, M. E. Kozlov, S. J. Kim, X. Xu, B. J. Swedlove, G. G. Wallace, R. H. Baughman, Artificial muscles from fishing line and sewing thread. *Science* **343**, 868–872 (2014).
7. S. Rosset, H. R. Shea, Flexible and stretchable electrodes for dielectric elastomer actuators. *Appl. Phys. A* **110**, 281–307 (2013).
8. K. Suzumori, S. Iikura, H. Tanaka, Flexible microactuator for miniature robots, in *IEEE Micro Electro Mechanical Systems* (IEEE, 1991), pp. 204–209.
9. T. A. Gisby, B. M. O'Brien, I. A. Anderson, Self-sensing feedback for dielectric elastomer actuators. *Appl. Phys. Lett.* **102**, 193703 (2013).
10. T. Helps, J. Rossiter, Proprioceptive flexible fluidic actuators using conductive working fluids. *Soft Robot.* **5**, 175–189 (2018).
11. Y.-L. Park, C. Majidi, R. Kramer, P. Bérard, R. J. Wood, Hyperelastic pressure sensing with a liquid-embedded elastomer. *J. Micromech. Microeng.* **20**, 125029 (2010).
12. B. Ward-Cherrier, N. Pestell, L. Cramphorn, B. Winstone, M. E. Giannaccini, J. Rossiter, N. F. Lepora, The tactip family: Soft optical tactile sensors with 3D-printed biomimetic morphologies. *Soft Robot.* **5**, 216–227 (2018).
13. M. Duranti, M. Righi, R. Vertechy, M. Fontana, A new class of variable capacitance generators based on the dielectric fluid transducer. *Smart Mater. Struct.* **26**, 115014 (2017).
14. R. Pelrine, R. Kornbluh, J. Eckerle, P. Jeuck, S. Oh, Q. Pei, S. Stanford, Dielectric elastomers: Generator mode fundamentals and applications. *Proc. SPIE Int. Soc. Opt. Eng.* **4329**, 148–156 (2001).
15. C. A. Aubin, S. Choudhury, R. Jerch, L. A. Archer, J. H. Pikul, R. F. Shepherd, Electroylitic vascular systems for energy-dense robots. *Nature* **571**, 51–57 (2019).
16. C. Horsman, S. Stepney, R. C. Wagner, V. Kendon, When does a physical system compute? *Proc. Math. Phys. Eng. Sci.* **470**, 20140182 (2014).
17. G. Dodig-Crnkovic, The info-computational nature of morphological computing, in *Philosophy and Theory of Artificial Intelligence, Studies in Applied Philosophy, Epistemology and Rational Ethics*, V. Müller, Ed. (Springer, Berlin, Heidelberg, 2013), pp. 59–68.
18. D. C. Horsman, Abstraction/representation theory for heterotic physical computing. *Phil. Trans. R. Soc. A* **373**, 20140224 (2015).
19. V. C. Müller, M. Hoffmann, What is morphological computation? On how the body contributes to cognition and control. *Artif. Life* **23**, 1–24 (2017).
20. G. Paun, *Membrane Computing: An Introduction* (Springer Science & Business Media, 2012).
21. R. Pfeifer, G. Gómez, Morphological computation–connecting brain, body, and environment, *Creating brain-like intelligence. Lecture Notes in Computer Science* **5436**, 66–83 (2009).
22. J. V. Neumann, *The Computer and the Brain* (Yale Univ. Press, 2012).
23. A. Adamatzky, *From Utopian to Genuine Unconventional Computers* (Luniver Press, 2006).
24. E. Fredkin, T. Toffoli, Conservative logic. *Int. J. Theor. Phys.* **21**, 219–253 (1982).
25. T. Toffoli, Reversible computing, in *International Colloquium on Automata, Languages, and Programming* (LIPIcs, 1980), pp. 632–644.
26. A. Adamatzky, Collision-based computing in Belousov–Zhabotinsky medium. *Chaos Soliton. Fract.* **21**, 1259–1264 (2004).
27. K. Morita, Reversible computing and cellular automata—A survey. *Theor. Comput. Sci.* **395**, 101–131 (2008).
28. S. Tsuda, S. Artmann, K. P. Zauner, The phi-bot: A robot controlled by a slime mould, in *Artificial Life Models in Hardware* (Springer, 2009), pp. 213–232.
29. T. Nakagaki, H. Yamada, Á. Tóth, Intelligence: Maze-solving by an amoeboid organism. *Nature* **407**, 470 (2000).
30. C. Isenberg, The soap film: An analogue computer: Soap films provide a simple method of obtaining analogue solutions to some mathematical problems. *Am. Sci.* **64**, 514–518 (1976).
31. E. Borré, J.-F. Stumbé, S. Bellemin-Laponnaz, M. Mauro, Light-powered self-healable metallosupramolecular soft actuators. *Angew. Chem. Int. Ed. Engl.* **55**, 1313–1317 (2016).
32. B. Florijn, C. Coulais, M. van Hecke, Programmable mechanical metamaterials. *Phys. Rev. Lett.* **113**, 175503 (2014).
33. R. Gatt, L. Mizzi, J. I. Azzopardi, K. M. Azzopardi, D. Attard, A. Casha, J. Briffa, J. N. Grima, Hierarchical auxetic mechanical metamaterials. *Sci. Rep.* **5**, 8395 (2015).
34. V. Braitenberg, *Vehicles: Experiments in Synthetic Psychology* (IT Press, 1986).
35. S. Nolfi, Power and the limits of reactive agents. *Neurocomputing* **42**, 119–145 (2002).
36. P. Fratzl, F. G. Barth, Biomaterial systems for mechanosensing and actuation. *Nature* **462**, 442–448 (2009).
37. M. Lévesque, É. Villiard, S. Roy, Skin wound healing in axolotls: A scarless process. *J. Exp. Zool. B Mol. Dev. Evol.* **314**, 684–697 (2010).
38. M. D. Ramirez, T. H. Oakley, Eye-independent, light-activated chromatophore expansion (LACE) and expression of phototransduction genes in the skin of *Octopus bimaculoides*. *J. Exp. Biol.* **218**, 1513–1520 (2015).
39. M. Cianchetti, T. Ranzani, G. Gerboni, T. Nanayakkara, K. Althoefer, P. Dasgupta, A. Menciassi, Soft robotics technologies to address shortcomings in today's minimally invasive surgery: The STIFF-FLOP approach. *Soft Robot.* **1**, 122–131 (2014).
40. A. D. Marchese, C. D. Onal, D. Rus, Autonomous soft robotic fish capable of escape maneuvers using fluidic elastomer actuators. *Soft Robot.* **1**, 75–87 (2014).
41. M. T. Tolley, R. F. Shepherd, B. Mosadegh, K. C. Galloway, M. Wehner, M. Karpelson, R. J. Wood, G. M. Whitesides, A resilient, untethered soft robot. *Soft Robot.* **1**, 213–223 (2014).
42. L. F. Cheow, L. Yobas, D.-L. Kwong, Digital microfluidics: Droplet based logic gates. *Appl. Phys. Lett.* **90**, 054107 (2007).
43. M. Prakash, N. Gershenfeld, Microfluidic bubble logic. *Science* **315**, 832–835 (2007).
44. M. W. Toepke, V. V. Abhyankar, D. J. Beebe, Microfluidic logic gates and timers. *Lab Chip* **7**, 1449–1453 (2007).
45. T. Thorsen, S. J. Maerkl, S. R. Quake, Microfluidic large-scale integration. *Science* **298**, 580–584 (2002).
46. T. Ranzani, S. Russo, N. W. Bartlett, M. Wehner, R. J. Wood, Increasing the dimensionality of soft microstructures through injection-induced self-folding. *Adv. Mater.* **30**, 1802739 (2018).
47. M. Wehner, R. L. Truby, D. J. Fitzgerald, B. Mosadegh, G. M. Whitesides, J. A. Lewis, R. J. Wood, An integrated design and fabrication strategy for entirely soft, autonomous robots. *Nature* **536**, 451–455 (2016).
48. S. T. Mahon, A. Buchoux, M. E. Sayed, L. Teng, A. A. Stokes, Soft Robots for Extreme Environments: Removing Electronic Control, in *IEEE Conference on Soft Robotics* (IEEE, 2019), pp. 782–787.
49. P. Zhu, L. Wang, Passive and active droplet generation with microfluidics: A review. *Lab Chip* **17**, 34–75 (2017).
50. B. Zhou, L. Wang, S. Li, X. Wang, Y. S. Hui, W. Wen, Universal logic gates via liquid-electronic hybrid divider. *Lab Chip* **12**, 5211–5217 (2012).
51. P. Rothemund, A. Ainla, L. Belding, D. J. Preston, S. Kurihara, Z. Suo, G. M. Whitesides, A soft, bistable valve for autonomous control of soft actuators. *Sci. Robot.* **3**, eaar7986 (2018).
52. D. J. Preston, P. Rothemund, H. J. Jiang, M. P. Nemitz, J. Rawson, Z. Suo, G. M. Whitesides, Digital logic for soft devices. *Proc. Natl. Acad. Sci. U.S.A.* **116**, 7750–7759 (2019).
53. S. Li, K. W. Wang, Fluidic origami with embedded pressure dependent multi-stability: A plant inspired innovation. *J. R. Soc. Interface* **12**, 20150639 (2015).
54. Y. Song, R. M. Panas, S. Chizari, L. A. Shaw, J. A. Jackson, J. B. Hopkins, A. J. Pascall, Additively manufacturable micro-mechanical logic gates. *Nat. Commun.* **10**, 882 (2019).
55. N. Chau, G. A. Slipher, B. M. O'Brien, R. A. Mrozek, I. A. Anderson, A solid-state dielectric elastomer switch for soft logic. *Appl. Phys. Lett.* **108**, 103506 (2016).
56. B. M. O'Brien, I. A. Anderson, An artificial muscle computer. *Appl. Phys. Lett.* **102**, 104102 (2013).
57. B. M. O'Brien, E. P. Calius, T. Inamura, S. Q. Xie, I. A. Anderson, Dielectric elastomer switches for smart artificial muscles. *Appl. Phys. A* **100**, 385–389 (2010).
58. B. M. O'Brien, T. G. McKay, S. Q. Xie, E. P. Calius, I. A. Anderson, Dielectric elastomer memory. *Electroact. Polym. Actuat. Devices* **7976**, 797621 (2011).
59. H. Hauser, A. J. Ijspeert, R. M. Füchslin, R. Pfeifer, W. Maass, Towards a theoretical foundation for morphological computation with compliant bodies. *Biol. Cybern.* **105**, 355–370 (2011).
60. E. Brown, N. Rodenberg, J. Amend, A. Mozeika, E. Steltz, M. R. Zakin, H. Lipson, H. M. Jaeger, Universal robotic gripper based on the jamming of granular material. *Proc. Natl. Acad. Sci. U.S.A.* **107**, 18809–18814 (2010).
61. M. Calisti, Soft robotics in underwater legged locomotion: From octopus–inspired solutions to running robots. in *Soft Robotics: Trends, Applications and Challenges*, *Biosystems & Biorobotics*, C. Laschi, J. Rossiter, F. Iida, M. Cianchetti, L. Margheri, Eds. (Springer, Cham, 2017), pp. 31–36.

62. S. Collins, A. Ruina, R. Tedrake, M. Wisse, Efficient bipedal robots based on passive-dynamic walkers. *Science* **307**, 1082–1085 (2005).
63. H. Hauser, A. J. Ijspeert, R. M. Füchslin, R. Pfeifer, W. Maass, The role of feedback in morphological computation with compliant bodies. *Biol. Cybern.* **106**, 595–613 (2012).
64. T. McGeer, Passive dynamic walking. *Int. J. Robot. Res.* **9**, 62–82 (1990).
65. K. Nakajima, H. Hauser, R. Kang, E. Guglielmino, D. G. Caldwell, R. Pfeifer, A soft body as a reservoir: Case studies in a dynamic model of octopus-inspired soft robotic arm. *Front. Comput. Neurosci.* **7**, 91 (2013).
66. R. Tedrake, T. W. Zhang, H. S. Seung, Learning to walk in 20 minutes, in *Proceedings of the Fourteenth Yale Workshop on Adaptive and Learning Systems* (2005), vol. 95585, pp. 1939–1412.
67. M. Garrad, J. Rossiter, H. Hauser, Shaping behaviour with adaptive morphology. *IEEE Robot. Autom. Lett.* **3**, 2056–2062 (2018).
68. H. Philamore, J. Rossiter, I. Ieropoulos, An energetically autonomous robotic tadpole with single membrane stomach and tail, in *Conference on Biomimetic and Biohybrid Systems*, (Springer, 2015), pp. 366–378.
69. S.-Y. Chang, K. Takashima, S. Nishikawa, R. Niiyama, T. Someya, H. Onodera, Y. Kuniyoshi, Design of small-size pouch motors for rat gait rehabilitation device. *Conf. Proc. IEEE Eng. Med. Biol. Soc.* **2015**, 4578–4581 (2015).
70. J. D. Greer, T. K. Morimoto, A. M. Okamura, E. W. Hawkes, Series pneumatic artificial muscles (spams) and application to a soft continuum robot. *IEEE Int. Conf. Robot. Autom.* **2017**, 5503–5510 (2017).
71. B. Kim, M. G. Lee, Y. P. Lee, Y. I. Kim, G. H. Lee, An earthworm-like micro robot using shape memory alloy actuator. *Sens. Actuators A Phys.* **125**, 429–437 (2006).
72. S. Seok, C. D. Onal, K.-J. Cho, R. J. Wood, D. Rus, S. Kim, Meshworm: A peristaltic soft robot with antagonistic nickel titanium coil actuators. *IEEE/ASME Trans. Mechatron.* **18**, 1485–1497 (2013).
73. A. Villanueva, C. Smith, S. Priya, A biomimetic robotic jellyfish (robojelly) actuated by shape memory alloy composite actuators. *Bioinspir. Biomim.* **6**, 036004 (2011).
74. R. Niiyama, X. Sun, C. Sung, B. An, D. Rus, S. Kim, Pouch motors: Printable soft actuators integrated with computational design. *Soft Robot.* **2**, 59–70 (2015).
75. M. Garrad, G. Soter, A. T. Conn, H. Hauser, J. Rossiter, Driving Soft Robots with Low-Boiling Point Fluids, in *IEEE Conference on Soft Robotics* (IEEE, 2019), pp. 74–79.
76. T. Umedachi, V. Vikas, B. A. Trimmer, Softworms: The design and control of non-pneumatic, 3D-printed, deformable robots. *Bioinspir. Biomim.* **11**, 025001 (2016).
77. T. Umedachi, B. A. Trimmer, Design of a 3D-printed soft robot with posture and steering control, in *IEEE International Conference on Robotics and Automation* (IEEE, 2014), pp. 2874–2879.
78. T. Umedachi, V. Vikas, B. A. Trimmer, Highly deformable 3D printed soft robot generating inching and crawling locomotions with variable friction legs, in *IEEE/RSJ International Conference on Intelligent Robots and Systems* (IEEE, 2013), pp. 4590–4595.
79. C. D. Onal, D. Rus, Autonomous undulatory serpentine locomotion utilizing body dynamics of a fluidic soft robot. *Bioinspir. Biomim.* **8**, 026003 (2013).
80. S. Seok, C. D. Onal, R. Wood, D. Rus, S. Kim, Peristaltic locomotion with antagonistic actuators in soft robotics, in *IEEE International Conference on Robotics and Automation* (IEEE, 2010), pp. 1228–1233.
81. T. Umedachi, K. Takeda, T. Nakagaki, R. Kobayashi, A. Ishiguro, Fully decentralized control of a soft-bodied robot inspired by true slime mold. *Biol. Cybern.* **102**, 261–269 (2010).
82. Z. E. Teoh, B. T. Phillips, K. P. Becker, G. Whittredge, J. C. Weaver, C. Hoberman, D. F. Gruber, R. J. Wood, Rotary-actuated folding polyhedrons for midwater investigation of delicate marine organisms. *Sci. Robot.* **3**, eaat5276 (2018).
83. K. Elgeneidy, P. Liu, S. Pearson, N. Lohse, G. Neumann, Printable soft grippers with integrated bend sensing for handling of crops, in *19th Annual Conference Towards Autonomous Robotic Systems* (2018), vol. 10965, pp. 479–480.
84. J. Guo, K. Elgeneidy, C. Xiang, N. Lohse, L. Justham, J. Rossiter, Soft pneumatic grippers embedded with stretchable electroadhesion. *Smart Mater. Struct.* **27**, 055006 (2018).
85. A. J. Ijspeert, A. Crespi, D. Ryczko, J.-M. Cabelguen, From swimming to walking with a salamander robot driven by a spinal cord model. *Science* **315**, 1416–1420 (2007).
86. H. Hauser, F. Corucci, Morphosis—Taking morphological computation to the next level, in *Soft Robotics: Trends, Applications and Challenges, Biosystems & Biorobotics*, C. Laschi, J. Rossiter, F. Iida, M. Cianchetti, L. Margheri, Eds. (Springer, Cham, 2017), pp.117–122.
87. A. M. Turing, On computable numbers, with an application to the entscheidungsproblem. *Proc. Lond. Math. Soc.* **s2-42**, 230–265 (1937).
88. A. J. Ijspeert, Central pattern generators for locomotion control in animals and robots: A review. *Neural Netw.* **21**, 642–653 (2008).
89. C. D. Onal, X. Chen, G. M. Whitesides, D. Rus, Soft mobile robots with on-board chemical pressure generation. *Robot. Res.* **100**, 525–540 (2017).
90. M. Wehner, M. T. Tolley, Y. Mengüç, Y.-L. Park, A. Mozeika, Y. Ding, C. Onal, R. F. Shepherd, G. M. Whitesides, R. J. Wood, Pneumatic energy sources for autonomous and wearable soft robotics. *Soft Robot.* **1**, 263–274 (2014).
91. C. Cao, X. Gao, A. T. Conn, A magnetically coupled dielectric elastomer pump for soft robotics. *Adv. Mater. Technol.* , 1900128 (2019).

Funding: This work was supported by the EPSRC Centre for Doctoral Training in Future Robotics and Autonomous Systems (FARSCOPE) EP/L015293/1. G.S. is supported by the EPSRC through DTP funding. J.R. is supported by EPSRC grants EP/M026388/1, EP/M020460/1, and EP/R02961X/1 and by the Royal Academy of Engineering as a chair in Emerging Technologies. H.H. is supported by Leverhulme Trust Project RPG-2016-345. A.T.C. is supported by EPSRC grants EP/P025846/1 and EP/R02961X/1. **Author contributions:** M.G., G.S., A.T.C., H.H., and J.R. jointly conceived of SMC and all device concepts. M.G. and G.S. designed experiments, manufactured devices, collected data, performed analysis, interpreted results, wrote the manuscript, and created movies. A.T.C., H.H., and J.R. advised on all parts of the project and reviewed manuscript. **Competing interests:** The authors declare that they have no competing interests. **Data and materials availability:** All data needed to support the conclusions of this paper are available in the paper or the Supplementary Materials. Additional data supporting this paper are available at the University of Bristol data repository: 10.5523/bris.2ld29myro7cvv2ismsbvgt6oun.

Submitted 28 March 2019
Accepted 29 July 2019
Published 21 August 2019
10.1126/scirobotics.aaw6060

Citation: M. Garrad, G. Soter, A. T. Conn, H. Hauser, J. Rossiter, A soft matter computer for soft robots. *Sci. Robot.* **4**, eaaw6060 (2019).

Science Robotics

A soft matter computer for soft robots

M. Garrad, G. Soter, A. T. Conn, H. Hauser, and J. Rossiter

Sci. Robot. **4** (33), eaaw6060. DOI: 10.1126/scirobotics.aaw6060

Science Robotics (ISSN 2470-9476) is published by the American Association for the Advancement of Science. 1200 New York Avenue NW, Washington, DC 20005. The title *Science Robotics* is a registered trademark of AAAS.